

T- Hop: A framework for studying the importance path information in molecular graphs for chemical property prediction.

Abdulrahman Ibraheem¹, Narsis Kiani^{1,2}, and Jesper Tegner¹

¹*KAUST, Saudi Arabia.*

²*Karolinska Institute, Sweden.*

Abstract

This paper studies the usefulness of incorporating path information in predicting chemical properties from molecular graphs, in the domain of QSAR (Quantitative Structure-Activity Relationship). Towards this, we developed a GNN-style model which can be toggled to operate in one of two modes: a non-degenerate mode which incorporates path information, and a degenerate mode which leaves out path information. Thus, by comparing the performance of the non-degenerate mode versus the degenerate mode on relevant QSAR datasets, we were able to directly assess the significance of path information on those datasets. Our results corroborate previous works, by suggesting that the usefulness of path information is dataset-dependent. Unlike previous studies however, we took the very first steps towards building a model that could predict upfront whether or not path information would be useful for a given dataset at hand. Moreover, we also found that, albeit its simplicity, the degenerate mode of our model yielded rather surprising results, which outperformed more sophisticated SOTA models in certain cases.

1 Introduction

Here, we study the importance of graph path information in predicting chemical properties from molecular graphs, a topic which falls under the topic of QSAR in the field of cheminformatics. For that purpose, we developed a framework called T-Hop which allows us to incorporate path information into a graph neural network (GNN) -style model. To allow us study the effect of path information, the framework comprises two modes: a non-degenerate mode which incorporates path information; and a degenerate mode which does not use path information. We applied the framework to six datasets from the MoleculeNet suite of cheminformatics datasets [21]. Results suggest that the effect of path information on accuracy is dataset-dependent. Also, we found no strong (Pearson) correlation between model performance and the maximum path length used in the model. Yet, we found that a degenerate case of our model yields positively surprising results on four out of the six datasets studied.

The present work’s application domain falls under the field of cheminformatics. Currently, the field of cheminformatics is witnessing great interest within the research community. This is due to a number of factors. First, cheminformatics has immense utility in the real world. For example, *de novo* drug design [1] [2], retrosynthesis frameworks [3], QSAR (Quantitative Structure-Activity Relationship) models [4], as well as molecular similarity and sub-structure matching tools [5], can relieve chemists and their parent pharmaceutical companies of a significant portion of the pain, energy, time and costs involved in the drug discovery and design process. Second, progress in the field of cheminformatics has been further fast-tracked by three favorable factors: 1) the increased availability of relevant cheminformatics data [6] [7] [8] [9] [10]; 2) the great strides recorded in machine learning, especially deep learning, which affords an avenue to extract useful information from the available data; and 3) the increased availability of compute and storage resources which supports the physical realization of the preceding two factors.

More specifically, this work focuses on datasets related to the branch of cheminformatics called QSAR [4]. QSAR is guided by the intuition that the observed physical, toxicological, physiological, and bioactivity-related properties of molecules are informed by the molecules’ underlying structures [12]. Approaches under QSAR include: 1) prediction of a target variable, such as aqueous solubility, from a compendium of calculable molecular descriptors [13] [14] [15] [16]; 2) the use of 2-d fingerprints [17] [18] [19] as inputs to a neural network or any other machine learning classifier; 3) the use of graph neural networks, which typically use primitive atomic features as inputs, with optional additional use of edge features and 3-d geometry information. [20] [21] [22] [23] 4) the use of smiles string as inputs in analogy with NLP models [24] [25] [26]; and 5) more recently, the use of the 2-d drawings/schematics of molecules [27], drawing inspiration from the field of computer vision.

Our T-Hop framework falls within the genre of graph neural networks (GNNs). For QSAR, GNNs represent molecules as graphs whose nodes are the atoms of the molecules, and whose edges are the bonds of the molecules. A unifying theme of most GNN-based models is that they compute neighborhood-aware representations for each node-centered neighborhood of the graph. In the context of molecules, this means computing embeddings for molecular sub-structures comprised of each atom and its neighboring atoms and bonds. The task of computing neighborhood-aware embeddings in GNNs has been approached in various ways in the literature. Generally, models differ in how they aggregate and combine information in the neighborhood of each node/edge. For example, some models use only node information [28] [29], whereas others blend node information with edge information [30] [31][20]. Also, some models use an attention mechanism [32] [33], while others jettison it altogether. Our T-Hop uses two pieces of information: node features and a linear combination of 2-d slices of a 3-d matrix containing path information.

2 Related work

T-Hop, being a GNN-style framework which incorporates path information, bears resemblance to several exiting GNNs that either implicitly or explicitly use path information. First, our framework is similar to IGCN [34] in the sense that the latter uses a powered symmetrically normalised identity-shifted adjacency matrix (PSNIA), which can ultimately be expressed in terms of the powered adjacency matrix, which in turn is known to contain path information. Moreover, the results of [34] are quite similar to ours, because in their experiments, utilizing path information does not yield better results in all cases. Further, Mix-Hop [35] also resembles our model because it also uses path information via the PSNIA. In fact, Mix-Hop involves a more extensive use of path information than IGCN, because it uses a set of PSNIAs with different powers, corresponding to different path lengths. Each layer of the model concatenates embeddings associated with different path lengths. While experiments in the Mix-Hop paper suggested that path information boosts accuracy, a more extensive set of experiments might ultimately show otherwise. Further, our framework also bears similarity to Power-Up [36] because the latter uses a matrix that records information about the path length of the shortest distance between all pairs of nodes in the graph in question. Similarly to [35], they consider a set of matrices, each associated with a specific shortest distance path length. However, unlike [35], they do not concatenate information across the matrices. Rather, similar to our approach, they use a learnable linear combination of the matrices.

Further, a line of works [37] [38] [39] [42] explicitly considers the sequence of paths leading to the nodes of a graph. In some cases, all paths are considered [42], while in some cases, shortest paths are considered [39], while in yet other cases, paths are sampled to lighten computational costs [38]. For example, in PathNet [38], path information is harnessed, with the aim of capturing graph global structure, especially in heterophily networks. They first sample paths using a maximal entropy path sampler, which takes the graph’s structure into consideration. Then using an LSTM-like cell, they compute node embeddings for target nodes by inputting the sequence of nodes on the target node’s path into the cell. To make the model distance-aware, a separate set of weights is learnt for each relevant distance. Experimental results showed that PathNet works better for heterophily graphs compared to homophily ones. Further, Geodesic graph neural nets (GDGNN) [37] seeks to improve on the expressiveness of GNNs, by incorporating so-called geodesic information, which essentially distills to pooling information along paths in the graph. In the GDGNN approach, a conventional GNN is first applied to the graph to compute embeddings for each node. So-called horizontal and vertical geodesics are then computed along relevant paths of the graph, by pooling embeddings along those paths. In the case of vertical geodesics, node degree and distance information are concatenated with the embeddings before pooling. A possible drawback is that the path associated with the horizontal pooling is chosen at random, to dodge high computational costs. However, this can lead to a situation wherein the pooling layer outputs different results for the same graph at different times. Moreover, experiments showed that GDGNN does not always outperform baseline methods. More recently, the

authors of PathNN[39] experimented with all paths between all pairs of nodes as well as with shortest paths, and put forth a theory that states that the set of all paths is more discriminatory than the 1-WL test. Similar to PathNet, they used an LSTM for modelling paths as distance-aware sequences of nodes (and edges). Their experiments showed that incorporating path information does not lead to better results in all cases.

Two aspects of Graphormer [41] also fit the above paradigm. First, in Graphormer, the shortest distance between every pair of nodes is used to augment the attention matrix. Second, the edges along the shortest path joining every pair of nodes is considered. Then the average of the dot products between each edge and a position-aware set of weights is computed and further used to augment the attention matrix. The above paradigm has also been extended to the domain of knowledge base completion. For example, in [42], following a compositional approach, they consider all paths between a source entity and a destination entity. For each path, they use an RNN to model the sequence of relations encountered from the source node to the destination node, with the goal of computing an output embedding that captures the direct relation between the source entity and the destination entity. A drawback of Path-RNN is that it considers all possible paths and this leads to huge computational costs .

Other works incorporating path information include NBFNet (Neural Bellman-Ford Networks) [43] and its special cases [45] [46] [47] . Inspired by the Bellman-Ford algorithm [44], NBFNet considers all paths between every pair of nodes in a graph. To alleviate computational complexity, they treat the paths in parallel, treating each path as a product of edges along the path. To cast the formulation unto a GNN setting, they used neural networks to: model the product of edges as a message passing function; and model the sum of paths as an aggregation function. Distinct advantages of NBFNet includes its suitability for both the transductive and inductive settings, as well as its modest computational complexity. However, unlike our framework, NBFNet focuses on link prediction rather than graph classification.

3 Introducing the T-Hop Framework

This section describes T-Hop, the framework we developed for studying the importance of path information for the domain of chemical property prediction from molecular graphs. Let $G = (V, E)$ represent a graph, where $V = \{v_1, \dots, v_n\}$ and $E = \{e_1, \dots, e_m\}$ are the nodes and edges of G , as usual. The adjacency matrix of G is A . We consider two arbitrary nodes, v_i and v_j in graph G . Let $\mathcal{B}_{i,j,k}^L$ be the number of paths of length L between v_i and v_j that contain v_k . Clearly, we can arrange the values, $\mathcal{B}_{i,j,k}^L$, in an $n \times n \times n$ 3-d tensor denoted $\mathcal{B}^L \in \mathbb{R}^{n \times n \times n}$, such that the entry on the i -th row, j -th column and k -th depth of \mathcal{B}^L is $\mathcal{B}_{i,j,k}^L$. Using $\mathcal{B}_{i,j,k}^L$, we now define a 3-d tensor, $\mathcal{T}^L \in \mathbb{R}^{n \times n \times n}$, as a scaled version of \mathcal{B}^L . Specifically, where $\mathcal{T}_{i,j,k}^L$ is the entry on the i -th row, j -th column and k -th depth of \mathcal{T}^L , we define $\mathcal{T}_{i,j,k}^L$ as follows:

$$\mathcal{T}_{i,j,k}^L = \frac{\mathcal{B}_{i,j,k}^L}{(L + 1)} \quad (1)$$

To proceed, we define a new $n \times n$ matrix \mathcal{M} as follows:

$$\mathcal{M} = \alpha_0 A + \sum_{L=2}^{L_m} \sum_{k=0}^{n-1} \alpha_{L,k} \mathcal{T}_{:::,k}^L \quad (2)$$

Above, A is adjacency matrix as usual, while α_0 and $\alpha_{L,k}$ are learnable scalars. Further, L_m is the maximum path length considered in the model, chosen due to computational considerations. Also, $\mathcal{T}_{:::,k}^L \in \mathbb{R}^{n \times n}$ is the 2-d matrix slice associated with depth- k of \mathcal{T}^L . We note from the above formula that \mathcal{M} is simply a learnt linear combination of the adjacency matrix, A , and depth- k slices of tensor \mathcal{T}^L . Using \mathcal{M} , the l -th layer of our T-Hop model can now be described as:

$$H^{l+1} = \sigma(\mathcal{M} H^l W^l) \quad (3)$$

Above, H^l denotes input features to the l -th layer, and W^l denotes a learnable matrix of weights, and $\sigma(\cdot)$ is a non-linear activation function. As usual, for the first layer of the network, we define $H^1 = X$ where $X \in \mathbb{R}^{n \times d}$ is the set of d -dimensional input features associated with the n nodes of the graph. Going back to Equation 2, we see that when the second term on the R.H.S of the equation is zero, we simply have $\mathcal{M} = \alpha_0 A$. When we use this value of \mathcal{M} in Equation 3, viz a viz $H^{l+1} = \sigma(\mathcal{M} H^l W^l)$, we call the resulting model a “degenerate model.” Importantly, it should be emphasized that the degenerate model does not use any path information at all. Rather, it only uses the adjacency matrix. Indeed, a centerpiece of this work is to empirically contrast the degenerate model with the non-degenerate model.

4 Connection between \mathcal{T}^L and the powered adjacency matrix.

On the one hand, the (i, j) entry of the powered adjacency matrix, A^L contains the number of paths of length L between nodes v_i and v_j , while on the other hand, the (i, j, k) entry of \mathcal{B}^L contains the number of paths of length L between v_i and v_j passing through v_k . Based on this, it is intuitive that a relationship should exist between A^L and \mathcal{B}^L . Moreover, given that $\mathcal{T}^L = \frac{\mathcal{B}^L}{(L+1)}$, it is also intuitive that a relationship should exist between A^L and \mathcal{T}^L . We now explore the connection between A^L and \mathcal{T}^L as follows. We start by defining the function, $f_{sum} : \mathbb{R}^n \rightarrow \mathbb{R}$, which simply outputs the sum of all components of its input vector. It can be shown that we would obtain the powered adjacency matrix, A^L , when we apply f_{sum} to \mathcal{T}^L . We first give the following definition:

Definition 4.1 (Cardinality of multiset \mathcal{P}^L). *Let G be a graph of nodes, $V = \{v_1, \dots, v_n\}$, and edges. Let v_i and v_j be any two arbitrary nodes in G , and Let A_{ij}^L be the number of simple paths of length L between v_i and v_j . Let $P_q^L = \{v_1^q, v_2^q, \dots, v_{L+1}^q\}$ denote the q -th simple path of length L between v_i and v_j , where v_k^q is the k -th node in the q -th path, P_q^L . Let $\mathcal{P}^L = \{P_1^L, P_2^L, \dots, P_{A_{ij}^L}^L\} = \{v_1^1, v_2^1, \dots, v_{L+1}^1, v_1^2, v_2^2, \dots, v_{L+1}^2, \dots, v_1^{A_{ij}^L}, v_2^{A_{ij}^L}, \dots, v_{L+1}^{A_{ij}^L}\}$ be a **multiset** containing all the simple paths of length L between v_i and v_j . **Then, the***

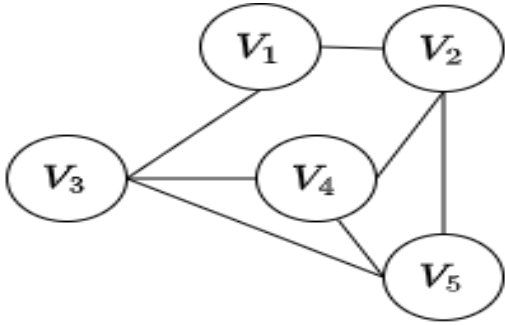


Figure 1: An illustrational graph of five nodes

cardinality of multiset \mathcal{P}^L is defined as the number of nodes in \mathcal{P}^L , counting multiplicities of nodes.

Based on the preceding definition, the following is a fact:

Fact 4.2 (Cardinality of multiset \mathcal{P}^L equals $\sum_k \mathcal{B}_{i,j,k}^L$). *The cardinality of multiset \mathcal{P}^L defined in Definition 4.1 above is equal to $\sum_k \mathcal{B}_{i,j,k}^L$*

Proof. The proof is best sketched with an example. As an example, let us use the graph G of five nodes depicted in Figure 1. Without loss of generality, let us consider all simple paths of length $L = 3$ between two arbitrary nodes, v_1 and v_5 in the graph. From the graph, we see that there are 2 simple paths of length 3 between v_1 and v_5 , so that $A_{1,5}^3 = 2$. These paths are $P_1^3 = \{v_1, v_2, v_4, v_5\}$ and $P_2^3 = \{v_1, v_3, v_4, v_5\}$. Hence, we may write $\mathcal{P}^3 = \{P_1^3, P_2^3\} = \{v_1, v_2, v_4, v_5, v_1, v_3, v_4, v_5\}$. Upon sorting \mathcal{P}^3 , we now have $\mathcal{P}^3 = \{v_1, v_1, v_2, v_3, v_4, v_4, v_5, v_5\}$. Now, given any node, v_k in G , when we count the multiplicity of v_k in the sorted version of \mathcal{P}^3 , we see it corresponds to the number of simple paths of length 3 between v_1 and v_5 that contain v_k . For example, we see clearly that node v_4 has multiplicity of 2, because it is contained in two different paths of length 3 between v_1 and v_5 , whereas node v_2 has multiplicity of 1, because it is contained in a single path of length 3 between v_1 and v_5 . Generalizing this observation, we see that, if \mathcal{P}^L is the multiset of nodes that constitute the simple paths of length L between any two arbitrary nodes, v_i and v_j , then for any node, $v_k \in \mathcal{P}^L$, the multiplicity of v_k in \mathcal{P}^L corresponds to the number of paths of length L between v_i and v_j that contain v_k , which in turn, by definition, is equal to $\mathcal{B}_{i,j,k}^L$. **In summary, for any node, $v_k \in \mathcal{P}^L$, the multiplicity of v_k in \mathcal{P}^L equals $\mathcal{B}_{i,j,k}^L$.** Based on this, we now consider the quantity $\sum_k \mathcal{B}_{i,j,k}^L$. It should be clear that the quantity $\sum_k \mathcal{B}_{i,j,k}^L$ simply equals the sum of multiplicities of all nodes in \mathcal{P}^L , which, in turn, equals the cardinality of \mathcal{P}^L . \square

Next, using Fact 4.2, we have the following proposition:

Proposition 4.3 (f_{sum} recovers A^L from \mathcal{T}^L). *Let $f_{sum} : \mathbb{R}^n \rightarrow \mathbb{R}$ be the function that takes a vector $u \in \mathbb{R}^n$ as input and returns as output the summation of all components of u . Then, with t_{ij}^L denoting the n -dimensional vector that stretches along the depth-axis*

of the 3-d tensor, \mathcal{T}^L , at a given i -th row, j -th column position of \mathcal{T}^L , we have that $f_{sum}(t_{ij}^L) = A_{ij}^L$.

Proof. To proceed, from Definition 4.1 above, we recall the meaning of the multiset $\mathcal{P}^L = \{P_1^L, P_2^L, \dots, P_{A_{ij}}^L\} = \{v_1^1, v_2^1, \dots, v_{L+1}^1, v_1^2, v_2^2, \dots, v_{L+1}^2, \dots, v_1^{A_{ij}}, v_2^{A_{ij}}, \dots, v_{L+1}^{A_{ij}}\}$; we also bring to mind the definition of the multiset’s cardinality given therein. In particular, the number of paths in \mathcal{P}^L is A_{ij} and each path contains $L + 1$ nodes, so that the cardinality of \mathcal{P}^L is equal to $(L + 1)A_{ij}^L$. Hence, we have $|\mathcal{P}^L| = (L + 1)A_{ij}^L$. But, we already know from Fact 4.2 above that $|\mathcal{P}^L| = \sum_k \mathcal{B}_{i,j,k}^L$. Hence, we have

$\sum_k \mathcal{B}_{i,j,k}^L = (L + 1)A_{ij}^L$, implying $\sum_k \frac{\mathcal{B}_{i,j,k}^L}{(L + 1)} = A_{ij}^L$. Further, by definition, we know

$\frac{\mathcal{B}_{i,j,k}^L}{(L + 1)} = \mathcal{T}_{i,j,k}^L$. Thus, $\sum_k \mathcal{T}_{i,j,k}^L = A_{ij}^L$. Now, it is clear that $\sum_k \mathcal{T}_{i,j,k}^L$ is tantamount to applying f_{sum} to the vector $t_{ij}^L = \mathcal{T}_{i,j,k}^L$, which completes the proof. \square

Proposition 4.3 reveals that T-Hop should be at least as expressive as a model that uses the sum of the adjacency matrix, A and the powered adjacency matrices, A^L . To see this, we begin with what the proposition says: $A_{ij}^L = \sum_k \mathcal{T}_{i,j,k}^L \implies \sum_{L=2}^{L_m} A_{ij}^L = \sum_{L=2}^{L_m} \sum_k \mathcal{T}_{i,j,k}^L \implies \sum_{L=2}^{L_m} A^L = \sum_{L=2}^{L_m} \sum_k \mathcal{T}_{:::,k}^L$. Now, if we restrict T-Hop by setting all the learnable parameters in Equation 2 to unity (i.e. setting $\alpha_0 = 1$, and $\alpha_{L,k} = 1$ for all L and k) then Equation 2 distills to $\mathcal{M} = A + \sum_{L=2}^{L_m} \sum_k \mathcal{T}_{:::,k}^L$, which makes it clear that $\mathcal{M} = A + \sum_{L=2}^{L_m} A^L$ under the restrictive setting that $\alpha_0 = 1$, and $\alpha_{L,k} = 1$ for all L and k . Hence, by removing this restriction, T-Hop is expected to be more expressive.

5 Experiments

We performed experiments in the domain of molecular property prediction [21] [59] [51]. By far, the most popular benchmark datasets in this domain are the MoleculeNet suite of datasets popularized by [21]. These datasets span both regression and classification tasks on the one hand, as well as single-task and multi-task classification problems on the other hand. Also, the authors of [21] considered four ways of splitting the datasets: random splitting, scaffold splitting, stratified splitting, and time splitting. In addition, some authors have also introduced a form of scaffold splitting called balanced scaffold splitting (e.g. [59]). For each dataset, the authors of [21], recommended a particular way of splitting the dataset in question. For example, for the ClinTox dataset [21], they recommend random splitting, whereas for the BBBP dataset [21], they recommend scaffold splitting. However, a more recent trend in the literature favors the jettisoning of the random splitting method, for the adoption of the scaffold splitting method. This trend is due to how the scaffold splitting method is better able to assess the generalization strengths of the proposed model/method. This is because the scaffold splitting method strives to make the molecules in the test set to be as different as possible from those in the training set. Thus, we focussed on the scaffold splitting method. Also, throughout our experiments, we adopted the standard 80:10:10 splitting for the training/validation/test

partitions of the datasets. We performed experiments on six datasets from the MoleculeNet suite of datasets. Three of the datasets (ClinTox, BACE and BBBP) involve classification tasks, while the other three (FreeSolv, ESOL and Lipophilicity) involve regression tasks. For the classification tasks, the pertinent metric is AUC-ROC, so that the higher the better, whereas for the regression tasks, the pertinent metric is R.M.S.E so that the lower the better. For each dataset, using a combination of automated hyperparameter search programs (such as TPE (Tree Parzen Estimator) from Optuna [54] and ASHA (Asynchronous Successive Halving Algorithm) from Ray Tune [55]), as well as hand-tuning, we searched for optimal hyper-parameters on the validation portion of the dataset. We chose the epoch that yielded best result on the test set. Following previous work, we ran randomly initialized models three times on each dataset, and recorded the mean and standard deviation of the runs. Our experiments were aimed at exploring four research questions. First, to see whether or not incorporating path information into our framework can yield significant gains in accuracy on the aforementioned datasets. Second, to see if there is a relationship between the maximum path length, L_m and accuracy. Third, given a dataset, to see if it is possible to predict upfront whether or not path information can yield gains in accuracy on the dataset. Fourth, to see how the framework compares with SOTA methods.

5.1 Juxtaposition of degenerate case against non-degenerate case and relationship between accuracy and maximum path length

It can be recalled from Section 3 that the T-Hop framework has two modes: 1). a non-degenerate mode which incorporates path information, and which corresponds to $L_m > 1$, where L_m is maximum path length; and 2) a degenerate mode which does NOT incorporate path information, and which corresponds to $L_m = 1$. Consequently, to explore whether or not incorporating path information into the framework leads to better performance or not, we juxtaposed the degenerate case with the non-degenerate case . We present the results in Table 1, where we see that path information increases accuracy on two out of the six datasets being considered. This suggests that incorporating path information does not always boost accuracy, and that, generally, the capability of path information to boost accuracies is dataset-dependent. Indeed, this observation aligns with experiments from some previous works [34]. For example, in the IGCN paper [34], experiments on the AWA2 dataset [50] showed worse performance as k increased from 1 to 3, where k can be viewed as a parameter that controls the maximum path length incorporated into the IGCN model. Likewise, in PathNN [39] whereas increasing path length improved results on the NCI1 dataset of the TUDataset collection [48], it failed to improve results on the PROTEINS and ENZYMES datasets of the same TUDataset collection. Moreover, even in recent work on dynamic graphs, viz GraphMixer [49] it was found that using a larger receptive field, and hence path length, diminished accuracies.

Further, we also conducted an experiment where we observed accuracies as L_m increased from 1 through 5 on each of the six datasets. We show results in Table 2. For each dataset, the last column of the table shows the Pearson correlations between performance measures and L_m . For the classification datasets (first three datasets), a

Table 1: Juxtaposition of Results for degenerate case ($L_m = 1$) against non-degenerate case ($L_m > 1$)

Dataset	Metric	Result for $L_m = 1$	Best Result for $L_m > 1$
BACE	ROC-AUC \uparrow	86.4 (0.003)	82.1(0.003)
BBBP	ROC-AUC \uparrow	73.5 (0.003)	70.0(0.037)
ClinTox	ROC-AUC \uparrow	91.2(0.017)	91.8 (0.015)
FreeSolv	R.M.S.E \downarrow	1.93 (0.132)	1.97(0.035)
ESOL	R.M.S.E \downarrow	0.90 (0.019)	0.96(0.017)
Lipophilicity	R.M.S.E \downarrow	0.74(0.016)	0.71 (0.010)

Table 2: Model performance across all values of L_m

Dataset	Metric	$L_m = 1$	$L_m = 2$	$L_m = 3$	$L_m = 4$	$L_m = 5$	Correlation
BACE	\uparrow	86.4	81.9	82.1	80.1	77.6	-0.95
BBBP	\uparrow	73.5	67.9	69.9	70.0	67.2	-0.68
ClinTox	\uparrow	91.2	88.1	89.6	89.6	91.8	0.29
FreeSolv	\downarrow	1.93	1.97	2.46	2.71	2.86	0.97
ESOL	\downarrow	0.90	0.93	0.96	1.00	1.03	0.99
Lipophilicity	\downarrow	0.74	0.71	0.71	0.71	0.74	0.12

high positive correlation would mean that incorporating path information boosts performance, while for the regression datasets (last three datasets) a high negative correlation would mean the same. However, as can be seen, we don't observe any such correlation values in the last column of the table, showing that increasing path length does not correlate strongly with performance boosts.

5.2 Towards upfront prediction of when path information helps

We now turn to the question of: given a dataset, can we contrive a way/rule to predict upfront whether or not path information would help on it? To motivate this question, we consider the compute times associated with computing A for $L_m = 1$, as well as \mathcal{T} and A for $L_m > 1$. We display the pertinent training compute times in Table 3. As expected the compute times increase as L_m increases. Considering this increase in compute times with L_m , it becomes important to ask: given a specific dataset, should we expend the extra computational effort of using $L_m > 1$ on it or not? Clearly, if we could contrive a rule to predict upfront that incorporating path information on a given dataset would not help, then we could save ourselves the extra compute time associated with using path information on that dataset, by simply using the degenerate mode of

Table 3: Single epoch training compute times in secs. across all values of L_m

Dataset	$L_m = 1$	$L_m = 2$	$L_m = 3$	$L_m = 4$	$L_m = 5$
BACE	1.09	10.13	22.09	35.54	50.69
BBBP	1.35	27.58	67.23	103.90	150.96
ClinTox	1.13	25.39	51.55	82.06	120.12
FreeSolv	0.59	0.70	0.82	0.93	1.09
ESOL	0.76	1.74	3.21	5.35	7.59
Lipophilicity	2.25	44.97	91.48	148.76	214.57

T-Hop. To forge ahead, we fell back on classical graph properties (e.g. graph diameter, closeness centrality, density, average clustering etc.). The idea is to use these properties as features in a machine learning classifier to make the aforementioned desired prediction. For each of the six datasets in this work, we computed fifteen such graph properties. However, because for some of the graph properties, we needed to compute: 1) means of node properties across the dataset 2) standard deviations of node property means across the dataset 3) mean of node property standard deviations across dataset, we ultimately arrived at a total of 36 features for each dataset. We show the computed properties in Tables 4, 5 and 6. Based on the preceding, for each of the six datasets, we computed a 36-dimensional feature vector. Hence, we got just 6 samples; each sample is 36-d vector associated with one of the six datasets. Towards building our predictor/classifier, we used the 3 samples associated with the 3 regression datasets as training samples, and used the remaining 3 samples as test samples. More specifically, we built a binary classifier trained to output 1 if the dataset associated with the input vector benefits from path information; otherwise, the classifier should output 0. Testing on the 3 test samples showed the classifier can successfully make accurate predictions on two of the three cases, thereby achieving a prediction accuracy of 66.67%. Thus, we see, given more datasets to train on, it is possible in principle to build a classifier that can predict upfront whether path information would be helpful on a given dataset. Of equal importance, this classification result also suggests that the classical graph properties used as features into the classifier offer significant explanation for why certain datasets benefit from path information, whereas others do not.

5.3 Comparing T-Hop with the SOTA

Looking back at Table 1, we see that the degenerate model performs better than the non-degenerate model on four out of the six datasets. It would therefore be instructive to compare the degenerate model with state-of-the-art models. We display the comparison in Table 7. The table shows that the degenerate model outperforms SOTA models on four out of the six datasets. Since the T-Hop framework does not incorporate 3-d geometry information, we limit the comparison in Table 7 to only SOTA models that also do NOT incorporate 3-d geometry information. However, despite the fact that these SOTA models do not incorporate 3-d information, some of them nonetheless utilize

Table 4: First five graph properties across all six datasets

Dataset	Path Info Helped ?	Node Degree	Max Weight Clique	Diam- eter	Density	Modu- larity
FreeSolv	NO	1.83	2.00	5.04	0.30	0.30
		0.28	0.11	2.11	0.16	0.14
		0.67				
ESOL	NO	1.98	2.01	7.02	0.22	0.39
		0.24	0.12	3.35	0.13	0.14
		0.72				
Lipophilicity	YES	2.18	2.05	13.85	0.09	0.60
		0.06	0.22	4.04	0.03	0.08
		0.69				
BACE	NO	2.17	2.10	15.22	0.07	0.65
		0.06	0.30	3.37	0.02	0.05
		0.76				
BBBP	NO	2.13	2.03	11.28	0.11	0.54
		0.14	0.16	4.18	0.07	0.10
		0.76				
ClinTox	YES	2.10	2.03	12.38	0.12	0.55
		0.17	0.18	6.01	0.09	0.13
		0.77				

Table 5: Next five graph properties across all six datasets

Dataset	Path Info Helped ?	Shortest Path Length	Closeness Centrality	Betweenness centrality	Edge Betw. centrality	Eigen-vector centrality
FreeSolv	NO	2.46	0.46	0.23	0.35	0.35
		0.74	0.15	0.07	0.14	0.11
			0.08	0.22	0.08	0.11
ESOL	NO	3.15	0.37	0.21	0.28	0.28
		1.13	0.14	0.06	0.12	0.10
			0.07	0.20	0.09	0.11
LIPOPHILICITY	YES	5.61	0.20	0.18	0.19	0.17
		1.40	0.06	0.02	0.02	0.03
			0.04	0.17	0.13	0.09
BACE	NO	6.29	0.17	0.17	0.17	0.14
		1.30	0.04	0.02	0.02	0.02
			0.03	0.18	0.14	0.10
BBBP	NO	4.70	0.24	0.18	0.20	0.19
		1.46	0.09	0.04	0.06	0.06
			0.05	0.17	0.12	0.10
ClinTox	YES	5.13	0.24	0.18	0.21	0.19
		2.15	0.11	0.04	0.08	0.08
			0.05	0.18	0.12	0.10

Table 6: Last five graph properties across all six datasets

Dataset	Path Info Helped ?	clustering coefficient	Smallest Laplacian eigenvalue	Second Smallest Laplacian eigenvalue	Second Largest Laplacian eigenvalue	Largest Laplacian eigenvalue
FreeSolv	NO	0.003	-6.26	0.36	3.52	4.53
		0.04	$4.21e^{-16}$	0.26	0.93	0.56
		0.002				
ESOL	NO	0.002	$-5.48e^{-17}$	0.25	4.11	4.87
		0.02	$5.25e^{-16}$	0.22	0.90	0.58
		0.003				
Lipophilicity	YES	0.004	$-2.11e^{-17}$	0.05	4.89	5.19
		0.02	$6.15e^{-16}$	0.05	0.24	0.22
		0.013				
BACE	NO	0.007	$4.44e^{-19}$	0.03	5.01	5.44
		0.02	$9.03e^{-16}$	0.02	0.19	0.23
		0.022				
BBBP	NO	0.003	$-4.06e^{-17}$	0.08	4.81	5.30
		0.03	$7.61e^{-16}$	0.10	0.56	0.38
		0.007				
ClinTox	YES	0.003	$2.16e^{-17}$	0.09	4.78	5.26
		0.03	$6.72e^{-16}$	0.14	0.62	0.38
		0.008				

Table 7: Comparison of the degenerate model with state-of-the-art models limited to 2-d information

Metric	ROC-AUC (Higher is better)			RMSE (Lower is better)		
	ClinTox	BBBP	BACE	FreeSolv	ESOL	Lipophilicity
DMPNN	90.6	71.0	80.9	2.082	1.050	0.683
AttentiveFP	84.7	64.3	78.4	2.073	0.877	0.721
N-GRAM _{RF}	77.5	69.7	77.9	2.688	1.074	0.812
N-GRAM _{XGB}	87.5	69.1	79.1	5.061	1.083	2.072
PretrainGNN	72.6	68.7	84.5	2.764	1.100	0.739
MolCLR	–	72.2	82.4	2.594	1.271	–
Grover _{base}	81.2	70.0	82.6	2.176	0.983	0.817
Grover _{large}	76.2	69.5	81.0	2.272	0.895	0.823
T-Hop	91.2	73.5	86.4	1.926	0.898	0.737

sophisticated mechanisms such as transformer-style aggregation as in GROVER [51] and AttentiveFP [22], whereas T-Hop does not. Moreover, some of the SOTA methods in Table 7, such as DMPNN [31], also incorporate edge features whereas T-Hop does not. Based on the foregoing it becomes imperative to ask: why should such a simple degenerate model outperform more sophisticated models like GROVER [51]? Well one possible answer can be obtained from the GraphMixer paper [49] wherein their simple model was shown to outperform more sophisticated models, such as DySAT [53] and JODIE [52], which incorporate transformer attention and RNNs. Hence, simpler models do not necessarily perform worse in all cases.

6 Conclusion

We have presented a study on the usefulness of incorporating path information in molecular graphs for the task of predicting chemical properties in the arena of QSAR. We designed a framework termed T-Hop which allowed us to effectively achieve this task on six datasets from the MoleculeNet suite of datasets. T-Hop afforded us an opportunity to study the importance of path information due to how it can be toggled to operate in one of two modes: a non-degenerate mode which incorporates path information and a degenerate mode which does NOT incorporate any path information. Consequently, by comparing T-Hop’s two modes on pertinent datasets we were able to evaluate the usefulness of path information on those datasets. Results showed that path information’s usefulness varies from dataset to dataset, an observation that aligns with results from previous work. But given that the usefulness of path information varies from dataset to dataset, we deemed it of value to explore avenues for predicting upfront whether or not path information would be useful on a given dataset. This is especially important because incorporating path information typically involves significantly extra computational overhead. Hence, we took the very first steps in this direction by building a classifier that can predict upfront whether or not path information would be useful on a given dataset. Finally, given that the degenerate version of our model performed better

than the non-degenerate version in most cases, we went on to compare that degenerate version with SOTA models. To our surprise we found that, despite its simplicity, the degenerate model outperforms SOTA models in certain instances.

References

- [1] Davide Crucitti, Carlos Pérez Míguez, Jose Ángel Díaz Arias, Diego Beltrán Fernández Prada and Adrián Mosquera Orgueira. De novo drug design through artificial intelligence: an introduction. *Frontiers in hematology*, 2024.
- [2] Liu, C., Korablyov, M., Jastrzebski, S., Włodarczyk-Pruszynski, P., Bengio, Y. and Segler, M. RetroGNN: Approximating Retrosynthesis by Graph Neural Networks for De Novo Drug Design. *Machine Learning for Molecules Workshop, NeurIPS*, 2020.
- [3] Xiangyan Sun, Ke Liu, Yuquan Lin, Lingjie Wu, Haoming Xing, Minghong Gao, Ji Liu, Suocheng Tan, Zekun Ni, Qi Han, Junqiu Wu, Jie Fan. ChemiRise: a data-driven retrosynthesis engine. *arXiv preprint arXiv:2108.04682*, 2021.
- [4] Srivastava, V., Selvaraj, C., Singh, S.K. . Chemoinformatics and QSAR. In: Singh, V., Kumar, A. (eds) *Advances in Bioinformatics*. Springer, Singapore (2021)
- [5] Hamid Safizadeh, Scott W. Simpkins, Justin Nelson, Sheena C. Li, Jeff S. Piotrowski, Mami Yoshimura, Yoko Yashiroda, Hiroyuki Hirano, Hiroyuki Osada, Minoru Yoshida, Charles Boone, and Chad L. Myers Improving Measures of Chemical Structural Similarity Using Machine Learning on Chemical–Genetic Interactions. *Journal of Chemical Information and Modeling* 2021 61 (9), 4156-4172
- [6] Bolton, E. E.; Wang, Y.; Thiessen, P. A.; Bryant, S. H. PubChem: Integrated Platform of Small Molecules and Biological Activities. *Annu. Rep. Comput. Chem.* 2008, 4, 217.
- [7] Huang, R.; Xia, M.; Sakamuru, S.; Zhao, J.; Shahane, S. A.; Attene-Ramos, M.; Zhao, T.; Austin, C. P.; Simeonov, A. Modelling the Tox21 10 K Chemical Profiles for in Vivo Toxicity Prediction and Mechanism Characterization. *Nat. Commun.* 2016, 7, 10425.
- [8] Kuhn, M.; Letunic, I.; Jensen, L. J.; Bork, P. The SIDER Database of Drugs and Side Effects. *Nucleic Acids Res.* 2016, 44 (D1), D1075–D1079.
- [9] Gaulton, A.; Hersey, A.; Nowotka, M.; Bento, A. P.; Chambers, J.; Mendez, D.; Mutowo, P.; Atkinson, F.; Bellis, L. J.; Cibrian-Uhalte, E.; Davies, M. The ChEMBL Database in 2017. *Nucleic Acids Res.* 2017, 45 (D1), D945–D954.
- [10] Schneider, G. Mind and Machine in Drug Design. *Nat. Mach. Intell.* 2019, 1 (3), 128–130.

- [11] Wang, Y.; Xiao, J.; Suzek, T. O.; Zhang, J.; Wang, J.; Zhou, Z.; Han, L.; Karapetyan, K.; Dracheva, S.; Shoemaker, B. A.; Bolton, E. PubChem’s BioAssay Database. *Nucleic Acids Res.* 2012, 40 (D1), D400–D412.
- [12] Carhart, R., Smith, D., Venkataraghavan, R. Atom pairs as molecular features in structure-activity studies: definition and applications. *J Chem Inf Comput Sci*, 25:64–73, 1985
- [13] Yap CW. PaDEL-descriptor: an open source software to calculate molecular descriptors and fingerprints. *J Comput Chem.*32(7):1466–1474, 2011.
- [14] Zhengguo C., Martina Z., Olanrewaju A., and Amanda H. Quantitative Structure–Activity Relationship (QSAR) Study Predicts Small-Molecule Binding to RNA Structure. *J Med Chem.* 65(10): 7262–7277, 2022.
- [15] Abdullahi, M., Uzairu, A., Shallangwa, G. A., Mamza, P. A., and Ibrahim, M. T. 2D-QSAR, 3D-QSAR, molecular docking and ADMET prediction studies of some novel 2-((1H-indol-3-yl)thio)-N-phenyl-acetamide derivatives as anti-influenza A virus. *Egyptian Journal of Basic and Applied Sciences*, 9(1), 510–532, 2022.
- [16] Aloui M, Er-Rajy M, Imtara H, Goudzal A, Zarougui S, El Fadili M, Arthur DE, Mothana RA, Noman OM, Tarayrah M, Menana E. QSAR modelling, molecular docking, molecular dynamic and ADMET prediction of pyrrolopyrimidine derivatives as novel Bruton’s tyrosine kinase (BTK) inhibitors. *Saudi Pharm J.*, 32(1):101911, 2024.
- [17] Venkatraman, V. FP-MAP: an extensive library of fingerprint-based molecular activity prediction tools. *Frontiers in Chemistry*, 2023
- [18] Tang, T., Song, D., Chen, J., Chen, Z., Du Y., Dang, Z., and Lu, G. Utilizing Machine Learning Models with Molecular Fingerprints and Chemical Structures to Predict the Sulfate Radical Rate Constants of Water Contaminants. *Processes* 12(2), 384, 2024.
- [19] Gao, K., Nguyen, D., Sresht, V., Mathiowetz, A., Tub, M. and Wei, G. Are 2D fingerprints still valuable for drug discovery? *Physical Chemistry Chemical Physics* 22(16), 2020.
- [20] Coley, C., Barzilay, R., Green, W., Jaakkola, T., Jensen, K. Convolutional Embedding of Attributed Molecular Graphs for Physical Property Prediction. *ACS Journal of Chemical Information and Modeling* 57, 8, 1757–1772, 2017.
- [21] Wu, Z., Ramsundar, B., Feinberg, E., Gomes, J., Geniesse, C., Pappu, A., Leswing, K., and Pande, V. MoleculeNet: a benchmark for molecular machine learning. *Chem. Sci.* 9, 513–530, 2018.
- [22] Xiong, Z., Wang, D., Liu, X., Zhong, F., Wan, X., Li, X., Li, Z., Luo, X., Chen, K., Jiang, H. and Zheng M. Pushing the Boundaries of Molecular Representation for Drug

- Discovery with the Graph Attention Mechanism. *Journal of Medicinal Chemistry*, 63 (16), 8749-8760, 2020.
- [23] Kearnes, S.; McCloskey, K.; Berndl, M.; Pande, V.; Riley, P. Molecular Graph Convolutions: Moving Beyond Fingerprints. *J.Comput.-Aided Mol. Des.* 30, 595, 2016.
- [24] Noutahi, E., Gabellini C., Craig M., Lim J. and Tossou, P. Gotta be SAFE: A New Framework for Molecular Design. arXiv preprint arXiv: 2310.10773, 2023.
- [25] Chithrananda, S., Grand, G. and Ramsundar, B. ChemBERTa: Large-Scale Self-Supervised Pretraining for Molecular Property Prediction. arXiv preprint arXiv:2010.09885, 2020.
- [26] Ross, J., Belgodere, B., Chenthamarakshan, V., Padhi, I., Youssef M., and Payel D., Large-scale chemical language representations capture molecular structure and properties. *Nat Mach Intell* 4, 1256–1264, 2022.
- [27] Zeng, X., Xiang, H., Yu, L. et al. Accurate prediction of molecular properties and drug targets using a self-supervised image representation learning framework. *Nat Mach Intell* 4, 1004–1016, 2022.
- [28] Gori M, Monfardini G, Scarselli F. A new model for learning in graph domains. In: *Proceedings. IEEE international joint conference on neural networks*, vol. 2, pp 729–734., 2005.
- [29] Kipf, T. and Welling, M. Semi-supervised classification with graphconvolutional networks, *ICLR*, 2017.
- [30] Gilmer, J., Schoenholz, S., Riley, P., Vinyals, O. and Dahl, G. Neural Message Passing for Quantum Chemistry. arXiv preprint arXiv:1704.01212, 2017.
- [31] Yang, K. Swanson K, Jin W et al. Analyzing learned molecular representations for property prediction. *J. Chem. Inf. Model.* 59, 3370–3388, 2019.
- [32] Veličković, P., Cucurull, G., Casanova, A., Romero, A., Liò, P. and Bengio, Y. Graph Attention Networks. *International Conference on Learning Representations*, 2018.
- [33] Shaked B., Uri A. and Eran Y. How Attentive are Graph Attention Networks? *International Conference on Learning Representations*, 2022.
- [34] Li, Q., Wu, X., Liu, H., Zhang, X., and Guan, Z. Label efficient semi-supervised learning via graph filtering. In *CVPR* 9582–9591, 2019.
- [35] Abu-El-Haija S., Perozzi B., Kapoor A., Harutyunyan H., Alipourfard N., Lerman K., Ver Steeg G., and Galstyan A. MixHop: Higher-Order Graph Convolutional Architectures via Sparsified Neighborhood Mixing, *ICML*, 2019.

- [36] Jin, M., Chang, H., Zhu, W., and Sojoudi, S. Power up! Robust Graph Convolutional Network via Graph Powering. AAAI, 2021.
- [37] Kong, L., Chen, Y., and Zhang, M. Geodesic Graph Neural Network for Efficient Graph Representation Learning. arXiv preprint arXiv:2210.02636, 2022.
- [38] Sun, Y., Deng, H., Yang, Y., Wang, C., Xu, J., Huang, R., Cao, L., Wang, Y., and Chen, L. Beyond Homophily: Structure-aware Path Aggregation Graph Neural Network. In Proceedings of the 31st International Joint Conference on Artificial Intelligence, pp. 2233–2240, 2022
- [39] Michel, G., and Nikolentzos, G., and Lutzeyer, J. and Vazirgiannis, M. Path Neural Networks: Expressive and Accurate Graph Neural Networks. Proceedings of the ICML, 2023.
- [40] Weisfeiler, B. and Lehmann, A. A reduction of a graph to a canonical form and an algebra arising during this reduction. Nauchno-Technicheskaya Informatsia, 2(9):12–16, 1968.
- [41] Ying, C., Cai, T., Luo, S., Zheng, S., Ke, G., He, D., Shen, Y., and Liu, T.-Y. Do Transformers Really Perform Bad for Graph Representation? In Advances in Neural Information Processing Systems, pp. 28877–28888, 2021.
- [42] Neelakantan, A., Roth, B., and McCallum, A. Compositional vector space models for knowledge base completion. In Proceedings of the ACL and IJCNLP, 156–166, 2015.
- [43] Zhu, Z., Zhang, Z., Xhonneux, L.P., Tang, J. Neural bellman-ford networks: a general graph neural network framework for link prediction. In: Advances in Neural Information Processing Systems, vol. 34, 2021.
- [44] Bellman, R. On a routing problem. Quarterly of applied mathematics, 16(1):87–90, 1958
- [45] Katz, L. A new status index derived from sociometric analysis. Psychometrika, 18(1):39–43, 1953.
- [46] Liben-Nowell, D. and Kleinberg, J. The link-prediction problem for social networks. Journal of the American society for information science and technology, 58(7):1019–1031, 2007.
- [47] Page, L., Brin, S., Motwani, R. and Winograd, T. The pagerank citation ranking: Bringing order to the web. Technical report, Stanford InfoLab, 1999.
- [48] Morris, C., Kriege, N. M., Bause, F., Kersting, K., Mutzel, P., and Neumann, M. TUDataset: A collection of benchmark datasets for learning with graphs. In Graph Representation Learning and Beyond Workshop, 2020.

- [49] W. Cong, S. Zhang, J. Kang, B. Yuan, H. Wu, X. Zhou, H. Tong, and M. Mahdavi. Do we really need complicated model architectures for temporal networks? In ICLR, 2023.
- [50] Xian, Y., Lampert, C., Schiele, B. and Akata, Z. Zero-shot learning—a comprehensive evaluation of the good, the bad and the ugly. *IEEE Transactions on Pattern Analysis and Machine Intelligence*, 2018.
- [51] Rong, Y. et al. Self-supervised graph transformer on large-scale molecular data. *Adv. Neural Inform. Process. Syst.* 33, 12559–12571, 2020.
- [52] Kumar, S., Zhang, X. and Leskovec, J. Predicting dynamic embedding trajectory in temporal interaction networks. In *Proceedings of the 25th ACM SIGKDD international conference on Knowledge discovery and data mining*. ACM, 2019.
- [53] Sankar, A., Wu, Y., Gou, L., Zhang, W. and Yang, H. Dysat: Deep neural representation learning on dynamic graphs via self-attention networks. In *Proceedings of the 13th International Conference on Web Search and Data Mining*, pp. 519–527, 2020.
- [54] Akiba, T., Sano, S., Yanase, T., Ohta, T., and Koyama, M. Optuna: A Next-generation Hyperparameter Optimization Framework. *KDD '19: Proceedings of the 25th ACM SIGKDD International Conference on Knowledge Discovery and Data Mining*, 2623–2631, 2019.
- [55] Liaw, R., Liang, E., Nishihara, R., Moritz, P., Gonzalez, J.E., and Stoica, I. Tune: A research platform for distributed model selection and training. *arXiv preprint arXiv:1807.05118*
- [56] Li, Q., Han, Z., and Wu, X. Deeper insights into graph convolutional networks for semi-supervised learning. In *Proceedings of the AAAI Conference on Artificial Intelligence*, volume 32, 2018.
- [57] K. Cho, B. van Merriënboer, D. Bahdanau, and Y. Bengio. On the properties of neural machine translation: Encoder-decoder approaches. *arXiv preprint arXiv:1409.1259*, 2014.
- [58] Vinyals O, Bengio S, Kudlur M. Order matters: sequence to sequence for sets. In: *International Conference on Learning Representations*, 2016.
- [59] Chen, J., Zheng, S., Song, Y., Rao, J. and Yang, Y. Learning attributed graph representations with communicative message passing transformer. *Proceedings of the Thirtieth International Joint Conference on Artificial Intelligence*, 2021.